



A rotating disk study of the photocatalytic oxidation of *p*-nitrophenol on phosphorus-modified TiO₂ photocatalyst



Daniel Méndez^{a,*}, Ronald Vargas^{a,*}, Carlos Borrás^a, Sergio Blanco^b, Jorge Mostany^a, Benjamín R. Scharifker^{a,c}

^a Departamento de Química, Universidad Simón Bolívar, Apartado 89000, Caracas 1080A, Venezuela

^b Centro de Tecnología de Materiales, Fundación Instituto de Ingeniería, Apartado 40200, Caracas 1040A, Venezuela

^c Universidad Metropolitana, Apartado 76819, Caracas 1070A, Venezuela

ARTICLE INFO

Article history:

Received 7 July 2014

Received in revised form 8 November 2014

Accepted 18 November 2014

Available online 3 December 2014

Keywords:

P-TiO₂

Rotating disk theory

Transport with surface reaction

Surface reactions

Heterogeneous photocatalysis

ABSTRACT

After discussing the general aspects of photocatalytic oxidation of organic compounds in aqueous solutions and the application of the rotating disk theory to (photo)catalytic phenomena, we report the oxidation of *p*-nitrophenol (PNP) on illuminated phosphorus modified TiO₂ (P-TiO₂) and TiO₂ photocatalysts under controlled hydrodynamic conditions. We found that the performance of the oxygen transfer reaction can be described considering mass transport in solution and surface reaction according to Langmuir–Hinshelwood kinetics. From analysis of the dependence of the reaction rate on the rotation rate, we obtained the apparent organic–photocatalyst adduct interaction constant *K*, the rate constant *k* of the surface reaction between adsorbed PNP and hydroxyl radicals, and the diffusion coefficient *D* of PNP in solution. The results showed that degradation of PNP using P-TiO₂ and UV light was readily possible, with reaction half-lives significantly lower than those obtained using pristine TiO₂ photocatalyst.

© 2014 Elsevier B.V. All rights reserved.

1. Introduction

Since Fujishima and Honda [1] reported in 1972 the UV-photoinduced water splitting at TiO₂ electrodes, there has been growing interest in the environmental applications of this semiconductor [2–10]. Heterogeneous photocatalysts based on TiO₂ materials have been developed as advanced oxidation processes for wastewater treatment, and these studies have shown that TiO₂/UV light photocatalysis have various advantages over other degradation methods. The catalyst is inexpensive and stable in a wide range of pHs and temperatures; the only reagents required for the oxidation process are oxygen and solar light; the method can be applied to a variety of organic pollutants in a wide range of concentrations; the oxidation process is not inhibited by intermediates or reaction products, it frequently leads to the complete mineralization of organic pollutants to CO₂ and, moreover, this advanced oxidation process may be combined with other methods of water treatment [5–8].

Under conditions of TiO₂/UV light photocatalysis, an electron from the TiO₂ valence band is promoted to the conduction band,

generating a hole in the valence band ($h\nu_B^+$) and an electron in the conduction band (e_{CB}^-). Adsorbed organics may react with holes in the valence band generating free radicals, and holes may be trapped by water or hydroxyl anions, generating hydroxyl radicals. On the other hand, electrons in the conduction band may react with dissolved oxygen to form the superoxide radical, leading to oxygen reduction to hydroxide by reaction with water. Radicals generated on the TiO₂ surface are highly reactive and generally promote the oxidation of organics via hydrogen abstraction or oxygen transfer from hydroxyl radicals to double bonds or aromatic rings. Recombination of charge carriers is an undesired process that determines the quantum conversion efficiency of the process [1–12].

In recent years efforts have been directed to solve two fundamental problems associated with TiO₂ photocatalysis. The first is increasing the sensitivity of TiO₂ to visible light, since the UV solar irradiance on the surface of the Earth is only 5% of the incident power, whereas the irradiance in the visible range amounts to ca. 50%. The second challenge is inhibiting the electron–hole recombination. Some examples of these efforts are the sensitization of semiconductors using organic molecules that absorb visible radiation [13–18], anchoring of “organic molecular wires” to extend the lifetime of photo-generated charge carriers [19], coupling of semiconductor systems [20,21], and modification of semiconductor nanostructures with metals [22–24] or non-metals [25–33].

* Corresponding author. Tel.: +58 212 906 3968; fax: +58 212 906 3969.

E-mail address: ronaldvargas@usb.ve (R. Vargas).

Non-metal modification of TiO₂ has attracted significant attention because of low fabrication costs of the photocatalysts and high efficiency relative to the conventional solid-state conversion of solar light into chemical energy [4,25–34]. However, the fundamental reasons for improvement have not been hitherto elucidated and are currently under investigation [35–37]. Lower band gaps and decreased recombination rates of charge carriers due to interactions with the elements incorporated into the crystal structure of the photocatalyst have been postulated as possible causes for the improved performance of TiO₂ modified with non-metals [4,25,35–37].

Modification of TiO₂ with phosphorus does not lead to enhanced visible light absorption due to band gap narrowing [27,33,37]; nonetheless greater UV-photoinduced catalytic effects have been observed on P-modified TiO₂ versus on pristine TiO₂ [4,25–27,33,37,38]. Thus incorporation of phosphorus species into the TiO₂ lattice has been of recent interest. Since changes in the properties of the semiconductor–electrolyte interface due to modification of TiO₂ with phosphorus and its effects on the electrochemical reactions occurring on its surface have not been as yet investigated, evaluation of the constant K of formation of the organic–photocatalyst adduct and the rate constant k of the surface reaction between the adsorbed organic and hydroxyl radicals would contribute to elucidate them.

The aim of the present study is to describe the kinetics of photocatalytic oxidation of *p*-nitrophenol on supported P-TiO₂. PNP adsorbs very strongly on the surface of TiO₂ and other metal oxides but its surface reaction with hydroxyl radicals occurs with low rates [39–42]; hence full description of the mineralization process requires resolving adsorption phenomena and the rate of surface reactions from the overall kinetics. For this purpose we used the recently developed theoretical model for processes involving adsorption–desorption and reaction on the surface of a rotating disk [40]. As shown below, the hydrodynamic method allowed resolving the apparent oxidation rate constants k_{obs} , describing the concentration decay of PNP in solution, into contributions due to adsorption and surface reaction on TiO₂ and P-TiO₂, respectively, and the results indicated that due to stronger adsorption and faster surface reaction rate, photooxidation of PNP occurs significantly faster on P-TiO₂ than on pristine TiO₂.

2. Applications of rotating disk theory to surface chemical reactions

Hydrodynamic techniques for the study of surface chemical reactions have been considered rigorously since the development of the rotating disk electrode (RDE) by Levich et al. [43,44]; the flux of matter is accurately controlled through the rotation rate and allowing precise quantification of the kinetic constant for the rate-determining step. Chemical kinetics models have been developed from the convective–diffusion equation, considering the hydrodynamic boundary layer theory that results from the solution of the Navier–Stokes and continuity equations, for appropriate geometries [43–46]. This theory has been developed for electrochemical reactions; therefore the kinetic models reported represent the electrical current (I) as a function of the rotation rate (ω) and the kinetic parameters of the chemical process. The analysis may extend as well to catalytic processes by virtue of the correspondence between the electric current and the reaction rate (dn_r/dt),

$$\frac{dn_r}{dt} = \frac{I}{nF} \quad (1)$$

The Levich equation [43] predicts that under totally mass transfer-controlled kinetics at the surface of a rotating disk, the

reaction rate is proportional to the square root of the rotation rate of the disk [43]:

$$\frac{dn_r}{dt} = 0.62AD^{2/3}\nu^{-1/6}\omega^{1/2}c \quad (2)$$

where A is the geometrical surface area of the catalyst disk, D is the diffusion coefficient of the reactant, c is its bulk concentration and ν is the kinematic viscosity of the solution.

Chemical reactions with comparable mass transfer and first order kinetic rates (with first-order heterogeneous reaction rate constant, k_h) at rotating disks have been analyzed by Koutecký and Levich [44]. In this case the linear dependence of dn_r/dt with $\omega^{1/2}$ breaks down and the Koutecký–Levich relation predicts that under mixed transport and first-order kinetics control, $(dn_r/dt)^{-1}$ is linearly related to $\omega^{-1/2}$:

$$\left(\frac{dn_r}{dt}\right)^{-1} = \left(\frac{k_h}{0.62Ak_hD^{2/3}\nu^{-1/6}c}\right)\omega^{-1/2} + \frac{1}{Ak_hc} \quad (3)$$

Recently, Vargas et al. [40] modified Levich-type relations in order to account for Langmuir–Hinshelwood (L–H) surface reactions. The diffusive–convective equation under hydrodynamic conditions appropriate for rotating disks was solved for surface reactions following the L–H kinetic mechanism, and an expression was obtained for the reaction rate as a function of rotation rate, considering mass transport, adsorption–desorption and slow reaction of adsorbed species on the catalyst surface:

$$\frac{dn_r}{dt} = \frac{A}{2K(1.61D^{1/3}\omega^{-1/2}\nu^{1/6})} \{DKc_0 + kK(1.61D^{1/3}\omega^{-1/2}\nu^{1/6}) + D - [(1.61D^{1/3}\omega^{-1/2}\nu^{1/6}kK + D - DKc_0)^2 + 4D^2Kc_0]^{1/2}\} \quad (4)$$

The reaction rate given by (4) is a nonlinear function of the rotation rate, with the surface reaction rate constant k , the adsorption constant K of the reactant on the catalyst, and the diffusion coefficient D of the reactant in solution, as parameters quantifying the kinetic phenomena. These parameters may be determined by non-linear fitting of (4) to experimental data, or through other appropriate graphical or numerical methods, described elsewhere [40]. The $(dn_r/dt)^{-1}$ vs. $\omega^{-1/2}$ representation of rotating disk data is suitable for studying the effect of surface reactions combined with mass transport [40]. Fig. 1 shows that Eqs. (2)–(4) have distinct and well-defined behaviors. In these coordinates, the Levich equation (2) describing purely mass transport-controlled kinetics is a straight line regressing to the origin. The Koutecký–Levich equation (3) describing mixed control by the rates of mass transport and reaction at the surface is also linear, but with a positive intercept inversely related to the reaction rate constant. In contrast, Eq. (4), describing mixed control by mass transport, adsorption, and surface reaction, shows non-linear behavior. At low rotation rates it approaches the linear behavior predicted by the Levich equation, but at faster rotation rates it tends to the limiting rate corresponding to the heterogeneous reaction rate of adsorbed chemical species at the catalyst surface.

The kinetic analysis can be extended to photocatalytic reactions; in these systems the L–H rate fits very well the organic compound degradation [3,6,47–51]. Ollis et al. [47,49] have shown that the L–H kinetic equation can be derived considering either adsorption equilibrium or steady state concentrations of adsorbed species, in this case, with the surface concentration of hydroxyl radicals continuously displaced from equilibrium depending on the intensity of illumination, and with L–H constants resulting exclusively from kinetic parameters.

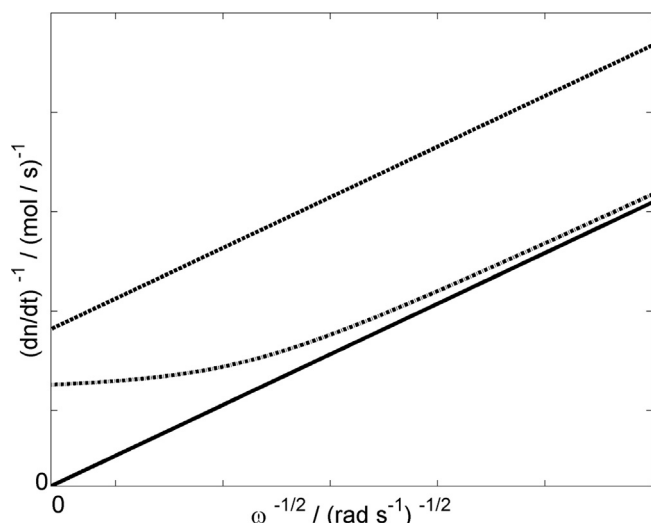


Fig. 1. $(dn/dt)^{-1}$ vs. $\omega^{-1/2}$ representation of reaction kinetics at rotating disk electrodes according to the Levich equation (—); Koutecký–Levich equation (---) and Eq. (4), corresponding to mass transport with adsorption and surface reaction (—•—).

3. Experimental

3.1. Instrumentation

Rotating disk experiments were carried out in a glass cell with quartz optical flat bottom, mounted on an optical-bench for irradiation from a Solar Light model LS 1000 UV solar simulator, fitted with a 1000 W xenon lamp to produce UV light at 290–400 nm. The radiation intensity was determined in each experiment using a Solar Light radiometer model PMA2100, while the rotation rate was controlled with a Pine Instrument model AFMSRX rotator. UV–vis spectra of the solution during catalytic oxidation of PNP were obtained with a Hewlett Packard model HP8452A diode array UV–Vis spectrophotometer under HP 89531 MS-DOS UV/VIS operating software. P-TiO₂ interactions were characterized using a Bruker model Tensor 27 Fourier transform infrared (FTIR) spectrometer, and the P/Ti ratio in the catalyst was determined from total reflection X-ray fluorescence (TXRF) spectra with multi-elemental analysis, obtained with a Bruker AXS model S2 PICOFOX analyzer. The crystal structure of the catalyst was determined with a Bruker model AXS D8 X ray diffractometer, using Cu-K α radiation. BET specific surface areas of the photocatalysts were determined using Quantachrome Nova 2000 nitrogen adsorption equipment. P-TiO₂ and TiO₂ UV–vis reflectance spectra were obtained with an Ocean Optics model S1024dw spectrometer, coupled with an Analytical Instruments Systems AIS model UV-2D light source and specular reflectance accessory with incidence at 90° (1/4" reflection probe model R200-7-UV/VIS). pH of solutions was recorded using a Hanna Instruments digital pH-meter, model P211, and intermediates formed during the reaction were identified with gas chromatography coupled with mass spectrometry (GCMS) using a Hewlett Packard model HP6890 gas chromatograph fitted with model HP5973 mass detector.

3.2. Synthesis and characterization of P-modified TiO₂ materials

Phosphorus-modified TiO₂ nanoparticles were synthesized according to the sol–gel method described elsewhere [25,34]. Titanium (IV) butoxide was used as titanium precursor, and phosphoric acid as phosphorus source. Synthesis was carried out following the procedure described by Lv et al. [27]. In the first stage, 30 μ l of 89% phosphoric acid, 10 ml of concentrated hydrochloric acid and

20 ml of ethanol were mixed to form a homogeneous solution. Then 4 ml of titanium butoxide and 4 ml of glacial acetic acid were dissolved in 20 ml of ethanol. Subsequently the solution prepared in the second step was kept at constant stirring while the solution prepared in the first step was dropped onto it over a period of 3 h, obtaining a stable and transparent colloid. After drying at 130 °C for 4 h, the powder obtained was sintered at 500 °C for 12 h to define the anatase crystal phase. Unmodified TiO₂ was prepared following the same procedure described above for P-TiO₂, without addition of phosphoric acid.

P-TiO₂ and TiO₂ thin films were respectively deposited onto 0.3 cm diameter disks of titanium using the spin-coating technique [52]. A high density suspension of the catalyst was prepared mixing 0.1 g of P-TiO₂ or TiO₂ powder with 1 M HCl, and placing it on the titanium substrate initially at 0 RPM and immediately driving it to 3300 RPM for 5 min; then the titanium disks with deposited P-TiO₂ or TiO₂ thin films were held at 120 °C for 15 min.

3.3. Photocatalytic oxidation of p-nitrophenol

The photocatalytic oxidation of PNP was studied at room temperature of 28 ± 1 °C in a one-compartment cell of 10 ml provided with an optically flat quartz window at the bottom, filled with an air-saturated 1.0 mM PNP + phosphate buffer (pH = 5) + 1.0 M Na₂SO₄ solution, prepared with synthetic grade PNP without further purification and analytical grade reactants, in ultrafiltered Nanopure® water with resistivity ≥ 18 M Ω cm. After placing them in solution, the P-TiO₂ or TiO₂ thin films on Ti disks were kept in the dark for 30 min at constant rotation speed to establish PNP adsorption/desorption equilibrium at the catalyst surface. Maintaining the same rotation speed, the system was then irradiated with ca. 30 mW cm⁻² UV light from the solar simulator, corresponding to typical solar UV power on a perfectly sunny day around noon [5]. The composition of the solution was determined extracting 100 μ l aliquots from the cell at different times. Intermediates formed during the reaction were identified with GCMS analysis after liquid–liquid extraction using dichloromethane as solvent [41]. The PNP and reaction products concentrations during oxidation were determined from UV–vis spectra of the 100 μ l aliquots, diluted to 10 ml with water, and deconvoluted using Matlab® v 7.0 software. Concentrations in solution were determined with the Lambert–Beer law with molar absorption coefficients at the wavelengths of maximum absorption for each compound [41,53]. Additionally, total organic matter during photocatalytic oxidation of PNP was established measuring the chemical oxygen demand (COD) according to the widely reported colorimetric method [54].

4. Results and discussion

4.1. Synthesis and characterization of P-TiO₂ and TiO₂ photocatalysts

Some features of the synthesized photocatalysts are shown in Fig. 2. The FTIR spectra shown in Fig. 2(A) confirm the presence of phosphorus in the P-modified TiO₂ catalyst; the broad 1033 cm⁻¹ band observed only in the P-TiO₂ sample is associated with the Ti–O–P asymmetric stretching, suggesting P atoms replacing Ti in the titania lattice [26,27]. The 3404 cm⁻¹ and 1632 cm⁻¹ bands observed in both P-TiO₂ and TiO₂ samples are associated to the stretching and bending vibrations modes, respectively, of the OH groups adsorbed at the interface [26]. From TXRF analysis, the P/Ti ratio in the P-TiO₂ catalyst was 1.14%, and the BET surface area was determined as 118 m² g⁻¹ and 96 m² g⁻¹ for P-TiO₂ and TiO₂, respectively; these values are consistent with data reported by Lv et al. [27] for their synthesis under similar conditions. Fig. 2(B)

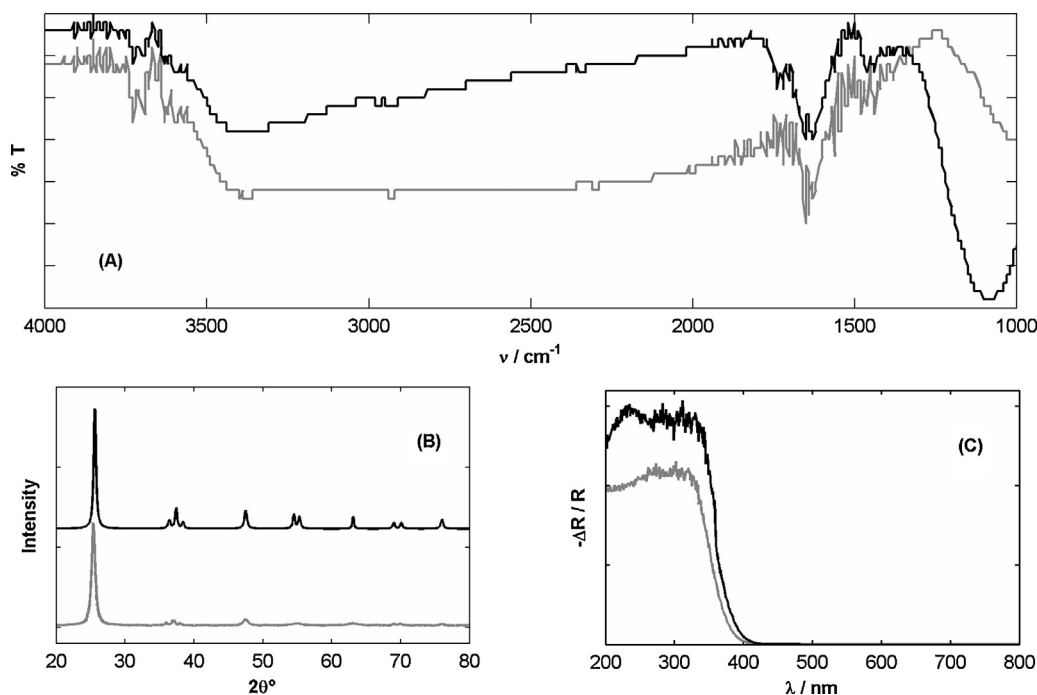


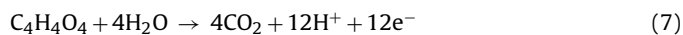
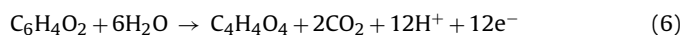
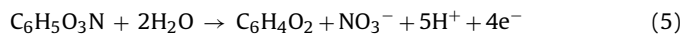
Fig. 2. FTIR spectra (A), XRD diffractograms (B) and UV–vis reflectance spectra (C) of P-TiO₂ (–) and TiO₂ (–) photocatalysts.

shows XRD diffractograms of both catalysts after calcination at 500 °C. The observed patterns match the anatase crystal structure, with crystallite size ca. 14 nm and ca. 20 nm for the P-TiO₂ and TiO₂ catalysts, respectively, estimated from the Scherrer equation. The UV–vis reflectance spectra of the photocatalysts are shown in Fig. 2(C). The band gaps of the synthesized P-TiO₂ and TiO₂ were 3.27 and 3.28 eV respectively, calculated from Kubelka–Munk theory [55,56], showing that the phosphorus modified sample did not redshift the band gap for absorption of visible sunlight radiation, consistent with previous experimental observations in phosphorus modified TiO₂ anatase without dye sensitization [27,33,57–59]. The stronger absorption in the UV range of the synthesized P-TiO₂ is also noteworthy; therefore the modified photocatalyst can take more advantage of the UV light in sunlight than the typically used TiO₂ semiconductor.

4.2. Photocatalytic oxidation of *p*-nitrophenol on P-TiO₂ and TiO₂ rotating disk photocatalysts

The degradation of phenolic compounds on TiO₂ nanoparticles has been studied previously [7,39,60,61] and it has been determined that efficient conversion to CO₂ occurred during UV irradiation. Fig. 3 shows the time evolution of UV–vis spectra during PNP photocatalytic oxidation on P-TiO₂ catalyst. The PNP absorption band with maximum at 318 nm decreases continuously, vanishing completely at sufficiently long times. Intermediates during reaction between PNP and hydroxyl radicals have been reported [41,42] and they also absorb in the UV; therefore, to determine the PNP concentration, it is necessary to deconvolute the contributions due to individual species from the experimental spectra [53]. The most stable intermediates reported during the oxidation of PNP are 1,4-benzoquinone and maleic acid, and their presence during photooxidation of PNP on TiO₂ and P-TiO₂ were verified with GCMS analysis. As shown in Fig. 3(B), the concentration of both intermediates first increased during photooxidation and then decreased until vanishing. This figure also shows the exponential decay of the PNP concentration after the initial stage of accumulation of intermediates. Thus considering only the most stable intermediates as

the major components during the process, the reaction path can be summarized as follows:



with charge balance provided by oxygen reduction at the catalyst surface:



Apparent pseudo-first-order kinetic constants (k_{obs}) for PNP oxidation were obtained from the slope of $\ln(c_{\text{PNP}})$ vs. t plots.

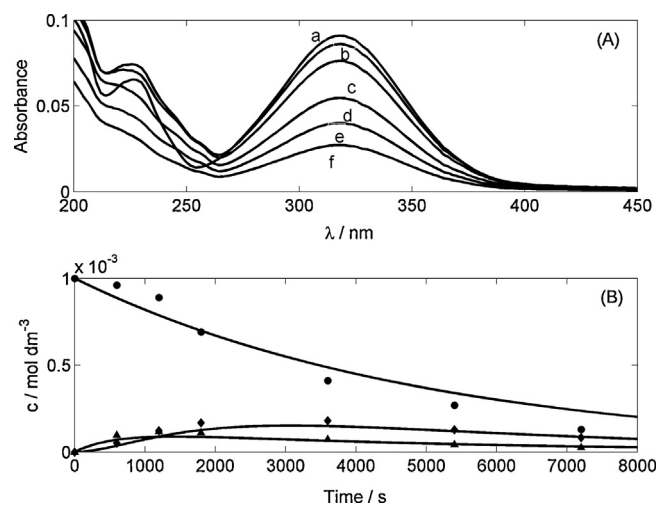


Fig. 3. (A) Absorption spectra during photocatalytic oxidation of *p*-nitrophenol on a P-TiO₂ catalyst disk rotating at 2500 rpm, recorded after 0 s (a), 20 s (b), 30 s (c), 60 s (d), 90 s (e) and 120 s (f) of solar irradiation at 30 mW cm⁻². (B) Concentrations of *p*-nitrophenol (●), benzoquinone (▲) and maleic acid (◆) during PNP oxidation under stated conditions, obtained from deconvolution of spectra such as those shown in (A). The curves represent the adjustment of the data to a first order consecutive reactions model.

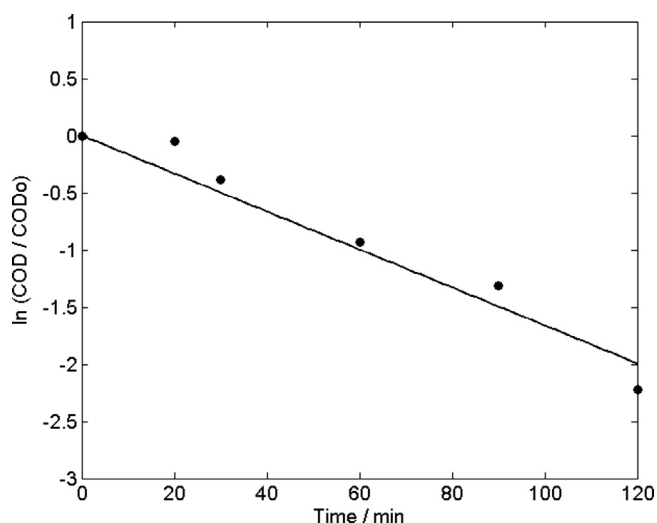


Fig. 4. $\ln(\text{COD}/\text{COD}_0)$ vs. time during photocatalytic oxidation of *p*-nitrophenol on a P-TiO₂ catalyst disk rotating at 2500 rpm.

Photocatalytic oxidation usually involves reaction of the organic compound on the semiconductor surface with hydroxyl radicals formed during water decomposition [3,6]. Depending upon the nature of the catalyst and the organic compound, the adsorbed states will determine the ultimate extent of the reaction and the oxidation rate [3,6,7,39,61]. Thus in order to associate the reaction constants measured with their respective chemical steps, it is essential to determine both the rate-limiting step and the extent of degradation. The chemical oxygen demand (COD) measures the total organic load susceptible to mineralization to CO₂ through oxidation [54]. Fig. 4 shows the COD decay during photocatalytic oxidation of PNP on P-TiO₂ and from the slope, the apparent pseudo-first-order rate constant $k_{\text{obs}}^m = 2.77 \times 10^{-4} \text{ s}^{-1}$ of the mineralization process was obtained. Under the same experimental conditions, the PNP photo-oxidation constant found from spectrophotometric measurements was $k_{\text{obs}} = 2.60 \times 10^{-4} \text{ s}^{-1}$. The proximity of both values indicates that mineralization and photocatalytic degradation take place under the same rate-limiting step [62] and without accumulation of stable intermediates. The apparent pseudo-first-order rate constants obtained for the photo-degradation of PNP on P-TiO₂ and TiO₂ rotating disk semiconductors at 2500 rpm are reported in Table 1, where reaction half-lives ($t_{1/2}$) estimated from the experiments and the PNP conversions ($X_{\text{PNP}}^{120'}$) at 120 min of reaction on each catalyst, are also reported.

4.3. Kinetic analysis of the surface reaction using rotating disk theory

Fig. 5 shows the PNP reaction rates as a function of rotation rate, in $(\text{dn}_r/\text{dt})^{-1}$ vs. $\omega^{-1/2}$ coordinates. The experimental data are well described by the behavior predicted for reaction rates limited by transport with adsorption and surface reaction, Eq. (4). At sufficiently slow rotation rates the reaction rate is limited by mass transport; under this condition Eq. (4) turns into the Levich

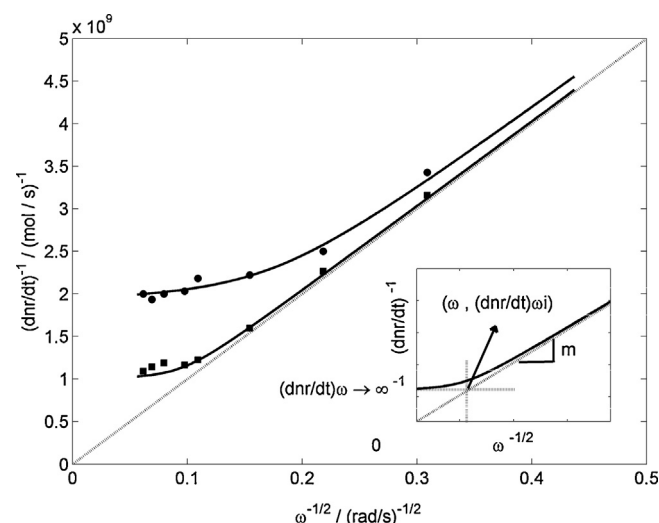


Fig. 5. Spectroscopically determined reaction rates $(\text{dn}_r/\text{dt})^{-1}$ vs. $\omega^{-1/2}$ for *p*-nitrophenol oxidation on (●) P-TiO₂ and (■) TiO₂ showing numerical fits of Eq. (4) to experimental data (—) and the Levich equation (.....). Inset: estimation of parameters m , $(\text{dn}_r/\text{dt})_{\omega_i}$ and $(\text{dn}_r/\text{dt})_{\omega \rightarrow \infty}$ used in Eqs. (10)–(12); see text and [40] for further details.

equation and the diffusion coefficient D can be estimated by evaluation of the slope $m = (0.62AD^{2/3}v^{-1/6}c)^{-1}$ of the straight line regressing to the origin in $(\text{dn}_r/\text{dt})^{-1}$ vs. $\omega^{-1/2}$ coordinates. At the opposite extreme of sufficiently fast rotation rates, the kinetics is controlled by the rate of the heterogeneous reaction; thus it does not depend on the rotation rate and is given by the apparent L-H rate law:

$$\left(\frac{\text{dn}_r}{\text{dt}}\right)_{\omega \rightarrow \infty} = \frac{AkKc_0}{1 + Kc_0} \quad (9)$$

where $(\text{dn}_r/\text{dt})_{\omega \rightarrow \infty}$ is the reaction rate at the limit of high rotation rates. The asymptotic behaviors corresponding to slow and to fast rotating rates intersect at a certain value of the rotation rate $\omega_i = [(\text{dn}_r/\text{dt})_{\omega \rightarrow \infty} / (0.62AD^{2/3}v^{-1/6}c)]^2$. Substituting the experimental reaction rate $(\text{dn}_r/\text{dt})_{\omega_i}$ at this rotation rate in (4) and solving the resulting expression together with the L-H Eq. (9) yields the adsorption constant K and the rate constant k . Hence D , K and k may be obtained from the following expressions [40]:

$$D = \left(\frac{1}{0.62Ac_m v^{-1/6}} \right)^{3/2} \quad (10)$$

$$K = \frac{(\text{dn}_r/\text{dt})_{\omega \rightarrow \infty} [2(\text{dn}_r/\text{dt})_{\omega_i} - (\text{dn}_r/\text{dt})_{\omega \rightarrow \infty}]}{c_0 [(\text{dn}_r/\text{dt})_{\omega \rightarrow \infty} - (\text{dn}_r/\text{dt})_{\omega_i}]^2} \quad (11)$$

$$k = \frac{(1 + Kc_0)(\text{dn}_r/\text{dt})_{\omega \rightarrow \infty}}{AKc_0} \quad (12)$$

The resulting values are reported in Table 2. The diffusion coefficient $D = 4.5 \times 10^{-6} \text{ cm}^2 \text{ s}^{-1}$ obtained is consistent with reported data [63,64] and the values for K and k for PNP decomposition on TiO₂ are also in agreement with data previously obtained with unsupported nanoparticles suspended in solution [39]. In order to compare the performance of the two photocatalyst we used the

Table 1

Kinetic parameters for oxidation *p*-nitrophenol on P-TiO₂ and TiO₂ catalysts at 2500 rpm: pseudo-first-order kinetic constants k_{obs} from PNP concentration decay and k_{obs}^m from COD, reaction half-life time $t_{1/2}$, and PNP conversion at 120 min $X_{\text{PNP}}^{120'}$.

Catalyst	$10^4 k_{\text{obs}}/\text{s}^{-1}$	$10^4 k_{\text{obs}}^m/\text{s}^{-1}$	$t_{1/2}/\text{s}$	$X_{\text{PNP}}^{120'}/\%$
P-TiO ₂	2.60	2.77	2420	87
TiO ₂	1.60	1.72	3910	71

Table 2

Langmuir–Hinshelwood constants for oxidation of *p*-nitrophenol on P-TiO₂ and TiO₂ catalysts.

	$10^{-7} K/\text{mol}^{-1} \text{ cm}^3$	$10^{10} k/\text{mol cm}^{-3} \text{ s}^{-1}$	$10^3 kK/\text{s}^{-1}$	$10^5 (kK/A_{\text{BET}})/\text{g s}^{-1} \text{ m}^{-2}$
P-TiO ₂	3.70	1.03	3.80	3.22
TiO ₂	1.60	0.55	0.87	0.90

maximum rate constant (kK) standardized with the BET area, this is shown in the Table 2, where is notable that the P-TiO₂ is a much better photocatalyst for the *p*-nitrophenol degradation. It should be noted that, in heterogeneous catalysis according to apparent Langmuir–Hinshelwood type kinetics, the pseudo first order constant is: $k_{app} = kK/(1 + Kc)$, then the real first order kinetic constant that serves to compare different reaction systems occurs when $Kc \ll 1$ and k_{app} results in kK values. For different catalyst surfaces standardization is necessary. The adsorption constant represents the magnitude of the organic compound–photocatalyst interaction, therefore their units should match inverse of concentration. The rotating disk analysis used to calculate these constants considered the normalizations indicated. Both the kinetic and the Langmuir–Hinshelwood apparent constants are significantly larger for P-TiO₂ than those for the unmodified TiO₂, making the overall degradation rate constant, $k_{obs} = kK/A_{BET}$, 3.58 times faster on P-TiO₂ than on the unmodified TiO₂. The increased catalytic efficiency for degradation of PNP, a very hazardous and hard to decompose organic compound, achieved by modification of the TiO₂ with phosphorus, makes P-TiO₂ a promising photocatalyst for decontamination of polluted water.

5. Conclusions

The photocatalytic activity of P-TiO₂ toward the degradation of *p*-nitrophenol was investigated supporting the photocatalyst on rotating disks and following the progress of mineralization with organic compound degradation techniques. The results were compared with analogous data obtained with unmodified TiO₂, and it was found that modification of TiO₂ with 1.14% phosphorus raised both the apparent equilibrium and the kinetic Langmuir–Hinshelwood constants 2.3 and 1.89 times, respectively, making the overall degradation rate constant, $k_{obs} = kK/A_{BET}$, 3.58 larger than that of the unmodified semiconductor. The synergistic effect of the Langmuir–Hinshelwood constants reduces the half-life of *p*-nitrophenol on illuminated P-TiO₂ to nearly one-half with respect to degradation on unmodified TiO₂, making P-TiO₂ a better material than the already excellent TiO₂, for degradation of organic contaminants dissolved in water.

Furthermore, this study proved the effective use of the rotating disk technique with the kinetic model based on transport with surface reaction [40], to evaluate the catalytic performance for decomposition of an organic compound with high adsorption on a photoactivated semiconductor.

Acknowledgements

We are grateful to the members of the Electrochemistry Group at Universidad Simón Bolívar for discussions.

References

- [1] A. Fujishima, K. Honda, *Nature* 283 (1972) 37–38.
- [2] D.F. Ollis, *Environ. Sci. Technol.* 19 (1985) 480–484.
- [3] M.R. Hoffman, S.T. Martin, W. Choi, D.W. Bahnemann, *Chem. Rev.* 95 (1995) 69–96.
- [4] X. Chen, S.S. Mao, *Chem. Rev.* 107 (2007) 2891–2959.
- [5] S. Malato, J. Blanco, D.C. Alarcón, M.I. Maldonado, P. Fernández-Ibáñez, W. Gernjak, *Catal. Today* 122 (2007) 137–149.
- [6] U.I. Gaya, A.H. Abdullah, *J. Photochem. Photobiol. C: Rev.* 9 (2008) 1–12.
- [7] R. Vargas, O. Núñez, *Sol. Energy* 84 (2010) 345–351.
- [8] D. Friedmann, C. Mendive, D. Bahnemann, *Appl. Catal. B: Environ.* 99 (2010) 398–406.
- [9] M.A. Henderson, *Surf. Sci. Rep.* 66 (2011) 185–297.
- [10] K. Nakata, T. Ochiai, T. Murakami, A. Fujishima, *Electrochim. Acta* 84 (2012) 103–111.
- [11] M.R. Fox, M.T. Dulay, *Chem. Rev.* 93 (1993) 341–357.
- [12] O. Carp, C.L. Huisman, A. Reller, *Progr. Solid State Chem.* 32 (2004) 33–177.
- [13] G. Mele, R. Del Sole, G. Vasapollo, E. García-López, L. Palmisano, M. Schiavello, *J. Catal.* 217 (2003) 334–342.
- [14] V. Iliev, *J. Photochem. Photobiol. A: Chem.* 151 (2002) 195–199.
- [15] V. Iliev, D. Tomova, L. Bilyarska, L. Prahov, L. Petrov, *J. Photochem. Photobiol. A: Chem.* 159 (2003) 281–287.
- [16] Z. Wang, W. Mao, H. Chen, F. Zhang, X. Fan, G. Qian, *Catal. Commun.* 7 (2006) 518–522.
- [17] R. Vinu, S. Poliseti, G. Madras, *Chem. Eng. J.* 165 (2010) 784–797.
- [18] P. Wen, S. Yang, Y. Ishikawa, H. Itoh, Q. Feng, *Appl. Surf. Sci.* 257 (2011) 2126–2133.
- [19] O. Núñez, C. Rivas, R. Vargas, *J. Phys. Org. Chem.* (2014) (in press).
- [20] M. Abou Asi, C. He, M. Su, D. Xia, L. Lin, H. Deng, Y. Xiong, R. Qiu, X.-Z. Li, *Catal. Today* 175 (2011) 256–263.
- [21] Z. Liu, X. Xu, J. Fang, X. Zhu, B. Li, *Appl. Surf. Sci.* 258 (2012) 3771–3778.
- [22] V. Iliev, D. Tomova, S. Rakovsky, A. Eliyas, G. Li Puma, *J. Mol. Catal. A: Chem.* 327 (2010) 51–57.
- [23] A. Zielinska-Jurek, E. Kowalska, J.W. Sobczak, W. Lisowski, B. Ohtani, A. Zaleska, *Appl. Catal. B: Environ.* 101 (2011) 504–514.
- [24] D. Tomova, V. Iliev, S. Rakovsky, M. Anachkov, A. Eliyas, G. Li Puma, *J. Photochem. Photobiol. A: Chem.* 231 (2012) 1–8.
- [25] A. Zaleska, *Recent Pat. Eng.* 2 (2008) 157–164.
- [26] R. Zheng, L. Lin, J. Xie, Y. Zhu, Y. Xie, *J. Phys. Chem. C* 112 (2008) 15502–15509.
- [27] Y. Lv, L. Yu, H. Huang, H. Liu, Y. Feng, *J. Alloys Compd.* 488 (2009) 314–319.
- [28] L. Szatmáry, S. Bakardjieva, J. Subrt, P. Bezduška, Z. Jirkovský, Z. Bastl, V. Brezová, M. Korenko, *Catal. Today* 161 (2011) 23–28.
- [29] L. Samiolo, M. Valigi, D. Gazzoli, R. Amadelli, *Electrochim. Acta* 55 (2010) 7788–7795.
- [30] Z. Zhang, X. Wang, J. Long, Q. Gu, Z. Ding, Z. Fu, *J. Catal.* 276 (2010) 201–214.
- [31] M. Behpour, V. Atouf, *Appl. Surf. Sci.* 258 (2012) 6595–6601.
- [32] H. Jiang, P. Yan, Q. Wang, A. Zang, J. Li, Q. Wang, *Chem. Eng. J.* 215–216 (2013) 348–357.
- [33] M. Iwase, K. Yamada, T. Kurisaki, O.O. Prieto-Mahaney, B. Ohtani, H. Wakita, *Appl. Catal. B: Environ.* 132–133 (2013) 39–44.
- [34] U.G. Akpan, B.H. Hameed, *Appl. Catal. A: Gen.* 375 (2010) 1–11.
- [35] X. Chen, C. Burda, *J. Am. Chem. Soc.* 130 (2008) 5018–5019.
- [36] A.V. Emeline, V.N. Kuznetsov, V.K. Rybachuk, N. Serpone, *Int. J. Photoenergy* (2008) 1–19 (Article ID 258394).
- [37] L. Körösi, I. Dékány, *Colloids Surf. A* 280 (2006) 146–154.
- [38] K. Elghni, O. Hentati, N. Mlaik, A. Mahfoudh, M. Ksibi, *J. Environ. Sci.* 24 (3) (2012) 479–487.
- [39] R. Vargas, O. Núñez, *J. Mol. Catal. A: Chem.* 300 (2009) 65–71.
- [40] R. Vargas, C. Borrás, J. Mostany, B.R. Scharifker, *Electrochim. Acta* 80 (2012) 326–333.
- [41] C. Borrás, C. Berzoy, J. Mostany, J.C. Herrera, B.R. Scharifker, *Appl. Catal. B: Environ.* 72 (2007) 98–104.
- [42] R. Vargas, C. Borrás, D. Plana, J. Mostany, B.R. Scharifker, *Electrochim. Acta* 55 (2010) 6501–6506.
- [43] V.G. Levich, *Physicochemical Hydrodynamics*, Prentice-Hall, Englewood Cliffs, NJ, 1962.
- [44] J. Koutecký, V.G. Levich, *Zh. Fiz. Khim.* 32 (1956) 1565.
- [45] A.J. Arvia, S.L. Marchiano, in: J.O'M. Bockris, B.E. Conway (Eds.), *Modern Aspects of Electrochemistry* No. 6, Plenum Press, New York, 1971, pp. 159–241.
- [46] A.J. Bard, L.R. Faulkner, *Electrochemical Methods: Fundamentals and Applications*, 2nd ed., John Wiley & Sons, New York, 2001.
- [47] C.S. Turchi, D.F. Ollis, *J. Catal.* 192 (1990) 178–192.
- [48] A.V. Emeline, V. Rybachuk, N. Serpone, *J. Photochem. Photobiol. A: Chem.* 8 (2000) 133.
- [49] D.F. Ollis, *J. Phys. Chem. B* 109 (2005) 2439–2444.
- [50] A. Mills, J. Wang, D.F. Ollis, *J. Phys. Chem. B* 110 (2006) 14386–14390.
- [51] B. Liu, X. Zhao, C. Terashima, A. Fujishima, K. Nakata, *Phys. Chem. Chem. Phys.* 16 (2014) 8751–8760.
- [52] D. Méndez, *Universidad Simón Bolívar, Caracas, (Chemical engineer dissertation)* 2013.
- [53] R. Vargas, C. Borrás, J. Mostany, B.R. Scharifker, *Water Res.* 44 (2010) 911–917.
- [54] A.L. Greenberg, A.E. Clesceri, *Standard Methods for the Examination of Water and Wastewater*, 18th ed., American Public Health Association, American Water Works Association, Waste Environment Federation, USA, 1992.
- [55] J.I. Pankove, *Optical Processes in Semiconductors*, Dover Publications, Inc., New York, 1971.
- [56] A.B. Murphy, *Sol. Energy Mater. Sol. Cells* 91 (2007) 1326–1337.
- [57] J.C. Yu, L. Zhang, Z. Zheng, J. Zhao, *Chem. Mater.* 15 (2003) 2280–2286.
- [58] L. Körösi, I. Dékány, *Colloids Surf. A* 280 (2007) 146–154.
- [59] L. Körösi, I. Dékány, *Chem. Mater.* 19 (2007) 4811–4819.
- [60] D. Chen, A.K. Ray, *Appl. Catal. B: Environ.* 23 (1999) 143–157.
- [61] E. Grabowska, J. Reszczynska, A. Zaleska, *Water Res.* 46 (2012) 5453–5471.
- [62] R. Vargas, S. Díaz, L. Viele, O. Núñez, C. Borrás, J. Mostany, B.R. Scharifker, *Appl. Catal. B: Environ.* 144 (2014) 107–111.
- [63] R. Niesner, A. Heintz, *J. Chem. Eng. Data* 45 (2000) 1121–1124.
- [64] S. Suresh, V.C. Srivastava, I.M. Mishra, *Chem. Ind. Chem. Eng. Q.* 19 (2013) 195–212.